CONTACT DEFECTS INITIATION IN RAILROAD WHEELS – EXPERIENCE, EXPERIMENTS AND MODELLING

Radim Halama[a,*], Rostislav Fajkoš[b], Petr Matušek[b], Petra Bábková[c], František Fojtík[a], Leo Václavek[a]

[a]Department of Mechanics of Materials, VŠB-Technical University of Ostrava, Ostrava, 17.listopadu 15, 708 33, Czech Republic

[b]Bonatrans Group, Bohumín, Revoluční 1234, 735 94, Czech Republic

[c]Centre of Advanced Innovative Technologies, VŠB-Technical University of Ostrava, Ostrava, 17.listopadu 15, 708 33, Czech Republic

* Corresponding author: tel. +420597321288, fax. +420596916490, radim.halama@vsb.cz

ABSTRACT

Main results of comprehensive research of rolling contact defects initiation are presented in this contribution. Description of own experimental study has been preceded by practical experience of a wheelset producer. A line rolling /sliding contact case with creepage of 0,75% was investigated using a unique test machine. The rail disc was made from Class C steel grade while the wheel disc from R7T steel grade. Unlike the standard twin-disc test, the diameter of the rail disc was 2.6 times bigger than the diameter of the wheel disc. Development of contact cracks and accumulation of shear strain for the wheel material R7T during rolling contact loading were namely evaluated. On the basis of test conditions, simulation by FEM was performed. As the result, very good prediction of shear strain accumulation was achieved using the AbdelKarim-Ohno cyclic plasticity model. The proposed computational strategy can be used for fatigue life prediction till initiation of a crack caused by low-cycle fatigue or by ratcheting failure.

Keywords: rolling contact fatigue, ratcheting, crack initiation, low-cycle fatigue

1 INTRODUCTION

Similarly as in the classical fatigue of materials, three stages can also be found in rolling contact fatigue (RCF) of the Wheel/Rail system, namely microcracks nucleation, crack initiation and crack growth. However, there are many differences between the classical multiaxial fatigue and the rolling contact fatigue (RCF) [1].

There are many research models for life prediction in the area of rolling contact fatigue [2]. Nevertheless, empirical approach has been the most frequently used approach in practise so far. In the empirical approach,

however, a lot of expensive tests must be realized in laboratory conditions with specimens that usually have similar or identical geometric proportions as the final product. Nowadays, new possibilities for testing of new materials on special test machines are introduced, however, test specimens are usually smaller and with different geometry, in order to cut costs. Therefore, wear resistance in rolling/sliding contacts is commonly evaluated through the twin-disc test [3], where cylindrical contact specimens with the same or nearly the same diameters are used.

In this way, examination was conducted with regard to wear and RCF for the most popular pearlitic and bainitic steel grades ([4], [5], [6]) under dry as well as wet rolling/sliding contact conditions. In terms of defects origination, it was found [7] that the dry rolling/sliding contact is more damaging for the initiation phase than the wet rolling/sliding contact. On the other hand, lubrication of the interfaces accelerates the crack propagation phase. Combination of both cases is then most damaging, when a block of dry rolling contact is followed by rolling under wet conditions [6]. The problem of fatigue crack propagation under lubricated rolling/sliding contact by utilizing the fracture mechanics was discussed in [8]. A crack model should take into account the effect of frictional locking between the faces of the crack and influence of fluid pressure acting on the crack faces [9].

Contact defects originate due to three main damage mechanisms: wear, RCF and ratcheting [10]. Loading applied on the rail by the railroad wheel can lead to accumulation of plastic deformation in the surface layer of the material - ratcheting. Tyfour and Beynon [11] realized twin-disc tests corresponding with typical wheel-rail contact conditions and they found that ratcheting, and not low-cycle fatigue, is the dominant damaging mechanism. Small surface cracks emerging already in the early stage of non-lubricated contact subsequently grow by shear mechanism, which confirms also the link between growth of surface cracks and wear rate [12].

In terms of costs savings, numerical methods appear to be a very perspective tool for durability assessment also for the area RCF. With respect to a big progress in criteria for low cycle and high cycle fatigue under non-proportional loading recently, many researchers seek to apply the same approaches for prediction of the number of cycles to crack initiation also in the field of rolling contact fatigue, see for instance [13] and [14]. No analytical solution is known in a general form for loads leading to cyclic plastic deformations, and numerical analysis is necessary for determination of stress-strain response. A complex plasticity model with higher number of parameters, which should be set using a number of experimental test data, is often required for correct description of material behaviour through numerical analysis. This applies namely in the case of significant friction forces during rolling, when cyclic creep (ratcheting) can occur. The ratcheting effect can be described as accumulation of any component of strain tensor with increasing number of cycles. It was found out by many researchers that cyclic plasticity models included in common commercial finite element programs (namely Besseling model and

Chaboche model) can not correctly describe ratcheting under non-proportional multiaxial loading [15]. The problem can be solved through implementation of a more complex cyclic plasticity model into the finite element program.

Ratcheting makes prediction of life to fatigue crack initiation difficult as the material could fail due to low-cycle fatigue or due to accumulation of a critical unidirectional plastic strain [16]. The previous study of Kapoor [17] which was conducted for various ductile materials subjected to uniaxial and biaxial loading conditions shows that ratcheting failure takes place when the accumulated strain reaches a certain critical value, and that ratcheting failure and low-cycle fatigue are independent failure mechanisms. It was also suggested that the critical strain level is close to the monotonic fracture strain. Under rolling/sliding conditions ratcheting occurs mainly as accumulation of shear strain. Ratcheting strain was experimentally investigated for example by Su and Clayton ([18], [19]) for pearlitic steel, but the specific value of critical strain for pearlitic steel was not analysed because of a lack of a sophisticated monitoring system to detect initial cracks with the crack sizes corresponding to microstructural phases.

This study begins with a description of defect types of railway wheelset and probable causes are discussed for chosen cases. A method of defects classification applied by a wheelset producer is also outlined. A series of tests under line rolling/sliding contact conditions was realized for the wheel made of R7T steel grade in order to study the crack initiation phase. In addition to mapping sizes and depths of characteristic defects based on metallographic investigation, accumulation of shear deformation at the depth of 0.15 mm for tests with numbers of cycles 500, 1000, 5000, 10000, 20000 and 60000 cycles was also examined. Consequently, a two-dimensional elastoplastic numerical analysis was carried out through the finite element method to simulate the rolling/sliding contact test and a pure rolling contact case. The rolling process was simulated by shifting normal and tangential stress distribution on the surface. Tangential forces were assumed to be proportional to the applied pressure, considering evolution of the friction coefficient measured in the realised experiment. Normal contact stresses were derived from a previous numerical analysis by the augmented Lagrangian method. The AbdelKarim-Ohno model, implemented into the finite element software Ansys and used in all performed analyses, predicts ratcheting of shear strain reasonably well for the rolling/sliding case. The low-cycle fatigue criterion of Jiang and Sehitoglu and the ratcheting criterion of Kapoor were applied for prediction of fatigue crack initiation. The analysis resulted in a surface crack prediction for the rolling-sliding case, where the ratcheting mechanism was recognised as the driving mechanism of crack initiation. In the pure rolling case is predicted, that the low-cycle fatigue causes subsurface crack initiation before the critical strain level is exceeded. Results correspond well with experimental investigation.

2 PRACTICAL EXPERIENCES

Main goal of wheelset producers is to achieve low wear of railroad wheels in relation to mileage. Railroad wheels for European customers are mainly manufactured from ER7, ER8 and ER9 steel grades (in accordance with EN 13262). The steels have pearlitic structure with ferrite content up to approximately 15% and having comparable hardness they reach higher wear resistance than steels with quenched and tempered structure, see Fig.1. Nevertheless, original pearlitic structure can be substantially modified depending on service conditions. For example, under shoe brake application in freight wagons, long-acting temperature of about 700°C can evoke the decrease of strength even after cooling to 20°C. At temperatures higher than 720°C material softening occurs during warming-up, but quenched structures can also arise in the cooling stage. Such quenched structures often originate due to malfunction of the wheel slide protection system or due to wrong brake regime settings. The wheel then slips on the rail inducing local heating up of a small part of the wheel tread, which is very quickly cooled by the relatively cold wheel-rim surroundings. In this way, quenched structures and corresponding damage occur.

The Fig.1 shows also different tendency to abrasive wear of structures produced by braking. Similarly like wheel tread damaging by repeated rolling contact loading, quenched structures have also negative influence on wear.

2.1 Service defect types of railroad wheels

A general catalogue of wheelset defects has been created under contribution of several authors of this paper [20], the purpose of which has been particularly unification of methodology for evaluation and classification of defects, specification of the critical defect size, and a guideline for a decision whether the wheel set can be further operated with the defined defect or whether it is necessary to reprofile it. At the present time, the catalogue has approximately 250 pages and a unique code number is assigned to every defect. Moreover, defect localization, its description and appearance, a method used for detection, probable cause of its origin, operational consequences of its occurrence, recommended repair method and defect photo documentation or its schematic representation are included. Selected defects from the catalogue that originate on wheelsets with different braking technology are presented in the table 1.

We will now illustrate description of examples of defects from the aforementioned catalogue that were also observed in samples from the experimental study presented in the next chapter.

2.2 Rolling of material over the rim outer face

Description and appearance:

Rollover of the wheel tread material surface layer in the direction from the tread contact circle to the outer rim face of the solid wheel, see Fig.2. In this way, lips develop around the wheel perimeter that are circle shaped. The defect can appear locally on a part of the wheel perimeter or on the whole perimeter. We can find this defect type generally on all wheels of a railroad vehicle operated under the same service conditions. The defect type can be dominant on wheelsets with higher axle loads.

Probable cause:

a) Due to acting of brake shoes, creepage etc. material surface layer substantially heats, thereby yield limit decreases with the growing temperature and the material creeps owing to cyclic loading of the wheel tread towards the rim face (Fig.3).

b) In consequence of sine movement of the wheel on the rail in lateral direction – lateral creepage

c) By virtue of railroad track (small curve radii)

2.3 Pitting - small loss of material from wheel tread

Defect localisation:

This type of defect can be indicated generally on all types of wheels and tyres, however, mainly on wheels braked by disc brake.

Description and appearance:

The defect has its typical morphology – disposition of tiny craters unevenly distributed on the wheel tread. Marginal size of craters does not exceed 5 mm with the depth from 0.2 to 0.7 mm. This defect occurs in the middle of the wheel tread. These defects in connection with small cracks signalise possible range of future crumbling away.

Defect detection method:

Visual control, possible fault replacing by „pock“ WR 211 (defect catalogue code).

Probable cause:

Pitting arises due to RCF (rolling contact fatigue) process caused by dynamic radial loading of wheels. Continuing

actuation of repeated contact loading can lead to pitting development (Fig. 4).

3 EXPERIMENTAL STUDY

3.1 Testing machine

A unique test machine TUORS (Technical University of Ostrava – Rolling Sliding wear testing machine) has been developed at the VŠB-Technical University of Ostrava during the last five years. The device was designed in order to simulate various wheel/rail contact cases. The experimental equipment is characterized by the normal loading force being applied statically by a weight through a lever mechanism, see Fig.5. The device is designed for maximal normal force of 12 kN. The driver and the follower are driven by a 2.2kW induction motor through several gear stages. Change of gears or appropriate selection of specimen diameters gives a slipping motion on the contact surface.

The usual ratio of specimen diameters is approximately 2.6. The direct driven specimen in the form of the rim (driver) has a double profile for economic reasons, and a next test can be realized after its reversion on other surface as can be seen at Fig. 6.

3.2 Experimental program

With the aim of life prediction technique development and closer investigation of the crack initiation stage of railroad wheels, a similar experimental program as that of Tyfour et al. [3] was realized. Using the described testing machine, the line rolling/sliding contact case close to real wheel/rail contact case was investigated. In reality, the rail curvature radius tends to infinity; in our case the rail diameter is much higher than the wheel diameter. The driver was made of Class C steel (Rail) and the follower of R7T steel (Wheel). Creepage of 0.75% was chosen, which was ensured by specimen diameter ratio slightly different from the cog wheels ratio in the gear box. The wheel disc diameter was 82.45 mm while the rail disc diameter was 215.55 mm. The initial contact line width was 8 mm. Rolling surface of each disc was ground to R_a roughness of 0.8 μm. The elastic Hertzian contact relevant to the maximum contact stress was about 1200 MPa. This fictitious pressure corresponded to the applied force of 9 kN. The surface contact area, determined by means of a pressure sensitive film, was 15 mm^2. Follower rotational speed was 280 revolutions per minute. All tests were non-stop tests. Individual wheel specimens were tested for 500, 1000, 5000, 10000, 20000 and 60000 rolling cycles.

The coefficient of traction was monitored during each test and mainly disc weight loss, disc diameter loss, hardness and surface roughness were investigated at the end of the tests. After sectioning of the specimen, the surface layer was prepared for metallographic observation in order to evaluate maximal defects and shear strain accumulation.

3.3 Main results of experiments

It is obvious from the previous text that the wheel discs were the object of interest. Due to this fact the test results are presented for specimens manufactured from R7T steel, unless otherwise indicated, see Tab. 2.
Surface degradation in relation to the number of cycles can be seen by naked eye at photographs of a part of specimens' contact surfaces corresponding to 1000, 5000, 20000 and 60000 cycles as presented at Fig. 7.
An area with average wear was chosen at each specimen. Surface photo-documentation performed by confocal microscope is also shown for mutual confrontation.
Roughness of individual specimens at the end of the test was measured in lateral direction by surface roughness tester. Pitting was measured after 60000 cycles by surface roughness tester as well, see Fig.8.
Measurement of the specimen diameter in the middle of specimen width was performed at the end of the test and cylindricity deviation was taken into account. Rollover lips were measured by image analysis. The torque at the coupling shaft between the wheel disc and gear box was measured. The overall friction force transferred in the contact surface was determined from the torque value and consequently the traction coefficient was calculated from the friction and normal force ratio. Dependence between the traction coefficient and the number of cycles is presented for the longest test at Fig. 9. Slow increasing of the traction coefficient (see Fig.10) during initial cycles corresponds with oxidative wear mechanism [3].
In the longest test, significant decrease of the traction coefficient from the value of 0.474 to 0.193 was observed (see Table 2). This phenomenon can be explained by decrease of the slip ratio in consequence of different abrasion of both specimens. The wheel disc diameter was reduced in relation to the number of cycles more rapidly than the rail disc diameter. At the following figure (Fig. 10), the starting part of this dependence for the test with 1000 cycles is apparent. The mentioned dependence is also used for description of friction coefficient variation in dependence on the number of cycles in the consequent simulation of the test– see the solid line at Fig. 10.
The instrumented indentation micro-hardness test according to the Vickers HV0.01 was performed for every specimen. The evaluated dependence between the micro-hardness and the distance from the contact surface is shown in the graph at Fig. 11. It is obvious from the graph that the highest hardening of the surface layer is

reached within the first 5000 cycles when the highest friction forces are reached.

3.4 Metallographic evaluation

Accumulation of shear deformation component with the number of cycles was apparent at photographs of etched specimens. The ratio of shear deformation mentioned in the Tab. 2 was measured through determination of angle tangent of grain boundary inclination [3] in the depth of 0.15mm. For lower numbers of cycles (500, 1000), pertinence of this method can be doubted due to the very small alternation of the grain boundary inclination angle as it is seen at Fig. 12.

At the other hand, this method can be reliably used for numbers of cycles over 5000 as it is apparent from the deformed microstructure displayed at Fig. 13.

Sizes and maximal depths of cracks in surface layer of all six not-etched specimens were investigated by a confocal microscope. Results of this investigation were already mentioned in Table 2.

Photographs were chosen from the obtained set that document well individual damage phases during rolling contact (Fig. 14). Defect development during the realized tests with creepage of 0.75 per cent can be described as follows:

1) Nucleation of first microcracks in the wheel discs was observed within the first 500 cycles.

2) Propagation of short cracks occurs in the next phase. Somewhere between 500 and 5000 cycles, a defect with a size at the limit of microstructure influence origins. Crack initiation occurs.

3) Macroscopic crack propagation follows, merging of cracks occurs which leads to creation of pitting (5000 – 60000 cycles).

Dependence between the maximal crack length and the number of cycles was depicted from the measurement results – see Fig. 15. Similarly, dependence between the maximal defect depth and the number of cycles is also characterized – see Fig. 16.

The crack depth remains approximately constant after about 30000 rolling passages. The shear strain was also measured at the crack tip and there was observed that it is almost independent on the cycles number. The mean shear strain value of 9.1 corresponds well with the results of Mazzú at el obtained for the same wheel steel [21].

4 PREDICTION OF CRACK INITIATION BY FEA

Research models of rolling contact fatigue require satisfactory description of stress-strain behaviour of the

material for further simulation of rolling contact. For the case of Wheel/Rail contact, an elastic-plastic stress analysis should be performed by a suitable numerical method. In this paper, the finite element method has been used, concretely performed through Ansys Release 11.0.

So called shakedown maps are mostly used [14] for estimation of material behaviour. On the basis of knowledge of the ratio of Hertzian pressure and shear yield stress p_0/k and of the traction coefficient f, it can be predicted whether elastic shakedown, plastic shakedown or ratcheting will occur. The shakedown map for the case of line rolling contact without assumption of slip is shown at Fig. 17. Two cases were chosen for the numerical study. The first one corresponds to the realized experiment for the rolling contact with forced slip of 0.75 per cent that was described in section 3. This case will be marked as the *RS case* (rolling/sliding). In this case, a variable traction coefficient was assumed. That is why this case is marked as a line in the shakedown map. The second case corresponds to the low value of traction coefficient f=0.05 and will be marked as the *FR case* (free rolling). The solved cases are in the area of plastic shakedown and ratcheting. A cyclic plasticity model suitable for ratcheting prediction should be considered.

4.1 Cyclic plasticity model

Progressive development of cyclic plasticity models in the last 20 years makes possible rather good description of material behaviour under proportional and non-proportional loading. The rolling contact belongs to the second mentioned group because principal stresses directions rotate during loading. The concept of yield surfaces is mostly used. From the ratcheting and cyclic plasticity point of view, the decisive factor is the kinematic hardening rule controlling the position of yield surface which marks limits of elastic behaviour. Time-independent incremental theory is considered with yield function $\bar{f}$ and von Mises yield criterion

$$\bar{f} = \sqrt{\frac{3}{2}(\mathbf{s}-\mathbf{a}) : (\mathbf{s}-\mathbf{a})} - \sigma_Y = 0 \,, \qquad (1)$$

where $\mathbf{s}$ is the deviatoric part of the stress tensor σ, $\mathbf{a}$ is the deviatoric part of the back-stress α and σ_Y is the initial size of the yield surface. Unfortunately, plasticity models included presently in commercial software packages are not able to describe ratcheting well [15]. The AbdelKarim-Ohno model [22] was used in this study. The model is characterised by the kinematic hardening rule

$$\mathbf{a} = \sum_{i=1}^{M} \mathbf{a}_i \,, \quad d\mathbf{a}_i = \frac{2}{3} C_i d\boldsymbol{\varepsilon}_p - \mu_i \gamma_i \mathbf{a}_i dp - \gamma_i H(f_i) \langle d\lambda_i \rangle \mathbf{a}_i \,, \qquad (2)$$

where $$f_i = \frac{3}{2}\mathbf{a}_i : \mathbf{a}_i - \left(\frac{C_i}{\gamma_i}\right)^2 \qquad (3)$$

and $$d\lambda_i = d\boldsymbol{\varepsilon}_p : \frac{\mathbf{a}_i}{C_i/\gamma_i} - \mu_i dp\,. \qquad (4)$$

In equation (2), the symbol $\langle . \rangle$ indicates the McCauley bracket, i.e. $\langle x \rangle = (|x|+x)/2$, dp and $d\varepsilon_p$ denotes equivalent plastic strain increment and plastic strain increment respectively. The parameters μ_i set a ratcheting rate. For simplification, only one parameter $\mu = \mu_i$ for all i is usually used in the AbdelKarim-Ohno model. The original AbdelKarim-Ohno model could simulate well only ratcheting in a stabilised state [22]. In addition, assuming the only one parameter for ratcheting $\mu = \mu_i$ and its evolution by equation

$$d\mu = \omega(\mu_\infty - \mu)dp \qquad (5)$$

transient effect in initial cycles is introduced [23]. In this paper, we consider six kinematic parts only ($M = 6$).

For model calibration and for fatigue behaviour investigation, a set of low-cycle fatigue tests was realized on specimens made from R7T steel under tension-compression and tension/torsion loading on the test machine MTS 858 MiniBionix at the CVUT in Prague. Deformations at the surfaces of testing parts were measured by an extensometer in the case of uniaxial test and by a strain-gauge bridge in the case of multiaxial test respectively. The details can be found in [24].

User-programmable feature had to be used to implement AbdelKarim-Ohno model into the Ansys Release 11.0, because the cyclic plasticity model is not included yet. The Fortran subroutine USERPL was improved for this purpose. The return mapping algorithm with successive substitution utilized by Kobayashi and Ohno [25] was used for implicit stress integration. By linking in own FORTRAN routine, a custom site-specific version of the ANSYS program was created and used for finite element analyses [26]. After compilation of source codes, all tasks with AbdelKarim-Ohno constitutive model take similar computing time as solutions with original models of Ansys program. A consistent tangent operator was derived for the assumed version of the AbdelKarim-Ohno model in the way published by Kobayashi and Ohno [25]. The convergence to the Newton-Raphson iteration for solution of the global system of nodal force equilibrium equations was then parabolic and much faster than that based on continuum tangent modulus.

The basic parameters σ_Y, $C_{1\text{-}6}$, $\gamma_{1\text{-}6}$ of the AbdelKarim-Ohno model and the elastic constants were determined from the stabilized hysteresis loop of the strain-controlled uniaxial test with deformation magnitude of 0.8 per cent – see Fig. 18 and Fig. 19 (case A). In this case, the empiric formulas mentioned by Bari and Hassan [15] were used. Parameters for ratcheting were determined using FEM so that the model may describe ratcheting well for the cases of both uniaxial and multiaxial loading. Detailed description of the model identification based on the uniaxial

ratcheting test is given by the author in [23]. The uniaxial ratcheting test was realized with the stress magnitude of 500 MPa and with the mean stress of 70 MPa. Accumulation of plastic deformation considered in the peaks of the opened hysteresis loops and the simulation results are shown at Fig. 20.

The multiaxial ratcheting test was performed for verification of the ascertained parameters. A loading path corresponding to loading of a point on the surface of a body loaded by rolling contact [27] was obtained by symmetric tension/compression and by mean torsion. A case with the axial stress magnitude of 490 MPa and the shear stress magnitude of 160 MPa was modelled. As a consequence of cyclic torsion of the specimen in one direction, increase of shear deformation in every cycle occurred. Dependence between the shear strain and the number of cycles obtained from the simulation corresponds well with the data obtained experimentally– Fig. 20. Prediction of the plastic deformation increment within one cycle is namely sufficient during the last cycles, which is obvious from the same trend of both curves.

In both ratcheting tests, there is apparent cyclic softening in initial cycles that is followed by the phase of cyclic hardening and by a stable state. Due to almost elastic behaviour of the material in the initial cycles, modelling of the initial cyclic softening is rather problematic. Respecting the fact that hundreds of cycles will be modelled within the rolling contact solution the cyclic softening was not included in the calculations.

4.2 Computational strategy

Two-dimensional elastoplastic finite elements analyses were carried out with linear elements PLANE42 under plane strain condition assumption. One thousand rolling cycles were simulated by shifting of normal and shear stresses distributions on the surface. The shear stresses were assumed to be proportional to the applied pressure. The normal contact stresses were derived from the previous numerical analysis by the augmented Lagrangian method. In this case only one rolling cycle was simulated. Contours of von Mises stress from the end of calculation are shown at Fig.21.

As it is apparent from the Fig.21 a function based on the Hertzian theory can be considered for further approximation

$$p(x) = \overline{p_0}\sqrt{1-\left(\frac{x}{a}\right)^2}\,, \qquad (6)$$

where a is half width of the contact area, x is the distance from the pressure peak and $\overline{p_0}$ represents the maximum of normal contact stresses from the elastoplastic analysis. The value of a must then correspond with the total normal force

$$F = \int_{-a}^{a} p(x)\,dx = \frac{\pi}{2}\overline{p_0}a\ . \qquad (7)$$

In the case of a soft slip as in this study, Coulomb's friction law can be applied for shear contact stress distribution

$$\tau(x) = f \cdot p\ , \qquad (8)$$

where f denotes the friction coefficient. It was determined by a numerical study [26] that using other function than (6) is more suitable for contact pressure description under high load factor value p_0/k. In both solved cases parameter values $\overline{p_0} = 1035MPa$ and $a = 0.77\text{mm}$ were assumed for stress distribution approximation.

In the auxiliary calculation, the friction coefficient 0.05 corresponding to the free rolling case was assumed for both solid cases (*RS* and *FR*). Variability of the friction coefficient was included only in the rolling/sliding case, according to the Fig.10. The AbdelKarim-Ohno model was assumed for the wheel disc as it was described in the previous section, while the Besseling multilinear kinematic model was used for the rail disc. In the second case the material model parameters corresponded to the cyclic strain curve of the Class C steel.

The proposed computational strategy for fatigue crack initiation prediction is apparent from the Fig.22. The phrase *material parameters identification* marks determination of constants of cyclic plasticity model as well as fatigue material parameters identification. It is assumed in this study that fatigue crack initiation as the consequence of low-cycle fatigue (LCF) occurs in the critical plane where the maximal value of the fatigue parameter proposed by Jiang-Sehitoglu is reached [2]

$$FP = \langle \sigma_{max} \rangle \frac{\Delta\varepsilon}{2} + J\Delta\gamma\Delta\tau\ , \qquad (9)$$

but only if exhaustion of the plastic material capacity does not occur earlier due to ratcheting of shear strain component as it was proposed by Kapoor [17].

Parameters σ_{max}, $\Delta\varepsilon$, $\Delta\gamma$, $\Delta\tau$ in the equation (9) mark the maximal stress, normal strain range, shear deformation range and shear stress range on the surveyed plane respectively and J is the parameter determined from the low-cycle fatigue torsion test.

It was further assumed that fatigue damage is accumulated linearly. Then the damage within one cycle caused by *LCF* can be expressed as follows

$$\frac{\mathrm{d}D_{LCF}}{\mathrm{d}N} = \frac{1}{N_{f,\,LCF}} = \frac{(FP - FP_0)^m}{K}\ , \qquad (10)$$

where FP_0, K and m are the material fatigue constants. Similarly, the damage caused by ratcheting is expressed as

$$\frac{\mathrm{d}D_R}{\mathrm{d}N} = \frac{1}{N_{f,\,R}} = \frac{\left|\mathrm{d}\gamma_R / \mathrm{d}N\right|}{\gamma_{cri}}\ , \qquad (11)$$

where γ_{cri} corresponds to the critical value of the accumulated shear strain which was determined on the basis of

the R7T material ductility.

The total ratcheting damage and the total fatigue damage are therefore defined as

$$D_R = \sum_1^N \frac{\mathrm{d}D_R}{\mathrm{d}N}, \quad D_{LCF} = \sum_1^N \frac{\mathrm{d}D_{LCF}}{\mathrm{d}N} \qquad (12)$$

and we assume that material fails, when one of those damages reaches unity. Within prediction, the values *FP* and $\mathrm{d}\gamma_R / \mathrm{d}N$ corresponding to the last simulation cycle were assumed for damage computation in cycles higher than 1000. All material parameters related to life-prediction and used in the calculations were determined experimentally for R7T steel and are mentioned in the Tab. 4.

4.3 Simulation results

Dependence between the accumulated shear strain and the number of cycles obtained in three chosen nodes is displayed at the Fig. 23. In the case of the Rolling/Sliding contact, there is an apparent passage from subsurface flow to surface flow as the consequence of friction coefficient increase, which corresponds well with the theoretical assumptions for the critical point passage when the transient value of friction coefficient 0.3 is reached – Fig. 17. For better understanding, the Fig. 10 and Fig. 23 can be compared. The ratcheting prediction result in the node located in the depth of 0.15 mm corresponds very well with experimental values as it is apparent from the Fig. 24. Results of the rolling contact fatigue life predictions of the number of cycles to the fatigue crack initiation are stated in the Table 5.

The used computational strategy led, in case of Rolling/Sliding contact, to prediction of number of cycles to a fatigue crack initiation of N_I= 1366. The initiation occurs at the surface layer as the consequence of ratcheting. A crack with the length of 154 μm corresponds to aforementioned number of cycles. The maximal grain size of investigated R7T wheel steel is about 30 μm. From an engineering point of view [14], influence of microstructure is suppressed in the case of cracks with lengths higher than 3-5 multiple of the characteristic grain size. Therefore the results of prediction correlate well to the experimental observations.

Experimental studies of Tyfour [3], Fletcher [12], Su [19] and also this one show that there is a critical value of shear strain, which can be accumulated in a surface layer and that stabilized growth of short surface cracks corresponds to the reaching the critical strain in deeper material layers. The constant wear rate accords to the moment when the crack tip attains an asymptotic value of crack depth [12]. In our experimental study the asymptotic value of the critical strain and the maximal crack depth are equal to 9.1 and 43μm respectively. Thus the number of cycles to constant wear rate conditions N_w can be calculated using the equation (11) and

considering γ_{cri} =9.1 for the R7T material. The value of the ratcheting rate $d\gamma_{xy}/dN$ calculated using FEM for the thousands cycle is equal to $2.949 \cdot 10^{-4}$ at the node placed 0.05 mm below the surface. It should be noted, that the node depth is close to the asymptotic value of crack depth. The assumption of linear extrapolation for ratcheting leads to the prediction of N_w=30858 cycles, which is in good correlation with conclusions of the section 4.3 and with the Fig.16.

5 CONCLUSIONS

Thanks to the used method good agreement with experimental data was achieved, both in the prediction of number of cycles to the fatigue crack initiation and ratcheting prediction in the case of rolling/sliding simulation. As shown in this paper, the cyclic plasticity model, which describes accumulation of shear strain reasonably well in the multiaxial ratcheting test proposed by McDowell [27], gives also realistic results when applied to rolling contact problems. The criterion of the maximal accumulated equivalent strain of Kapoor [17] is useful also from the practical point of view, because there is a critical value of strain, when the material shows steady wear behaviour [3]. On the other hand, results of crack initiation prediction are very sensitive to the critical strain value. In this paper, it was considered that it corresponds with the ductility of material. In a future work, more experimental efforts are needed for the critical strain value estimation.

In order to perform the whole life prediction, it is necessary to extend the computational strategy by modelling of fatigue crack propagation using an approach of the elasto-plastic fracture mechanics. Interesting works in this field are for example [28] and [29].

Acknowledgement

This research has been supported by the project MSM6198910027 of the Ministry of Education, Youth and Sports of the Czech Republic. Authors would like to appreciate the assistance of BONATRANS GROUP a.s. Bohumin company during the preparation and realization of experiments and documentation support throughout the article preparation.

References

[1] A. Ekberg, E. Kabo: Fatigue of railway wheels and rails under rolling contact and thermal loading—an

overview. *Wear* 258 (7-8) (2005), pp. 1288-1300.

[2] Y. Jiang, H. Sehitoglu: A model for rolling contact failure. *Wear* 224 (1) (1999), pp. 38-49.

[3] W.R. Tyfour, J.H. Beynon, A. Kapoor: The steady state wear behaviour of pearlitic rail steel under dry rolling-sliding contact conditions. *Wear* 180 (1-2) (1995), pp. 79-89.

[4] P. Clayton, D.N. Hill: Rolling contact fatigue of a rail steel. *Wear* 117 (1987), pp. 319-334.

[5] J.E.Garnham, J.H. Beynon: Dry rolling-sliding wear of bainitic and pearlitic steels. *Wear* 157 (1992), pp. 81-109.

[6] D.I. Fletcher, J.H. Beynon: The effect of contact load reduction on the fatigue life of pearlitic rail steel in lubricated rolling-sliding contact. *Fatigue & Fracture of Engineering Materials & Structures* 23 (2000), pp. 639-650.

[7] W.R. Tyfour, J.H. Beynon, A. Kapoor: Deterioration of rolling contact fatigue life of pearlitic rail steel due to dry-wet rolling-sliding line contact. *Wear* 197 (1996), pp. 255-265.

[8] M. Kaneta, H. Yatsuzuka, and Y. Murakami: Mechanism of crack growth in lubricated rolling/slidding contact. *ASLE Trans.* 28 (3) (1985), pp. 407–414.

[9] A.F. Bower: The influence of crack face friction and trapped fluid on surface initiated rolling contact fatigue cracks. *J. Tribol., Trans. ASME*. 110 (4) (1988), pp. 704–711.

[10] C. Boher, O. Barrau, R. Gras, F. Rezai-Aria. A wear model based on cumulative cyclic plastic straining. *Wear* 267 (5-8) (2009), pp. 1087-1094.

[11] W.R. Tyfour, J.H. Beynon: The effect of rolling direction reversal on the wear rate and wear mechanism of pearlitic rail steel. *Tribology International* 27 (1994), pp. 401-412.

[12] D.I. Fletcher, J.H. Beynon: Equilibrium of crack growth and wear rates during unlubricated rolling-sliding contact of pearlitic rail steel. *Proceedings of the Institution of Mechanical Engineers* 214 (2000), pp. 93-105.

[13] A. Bernasconi, P. Davoli, M. Filippini, S. Foletti. An integrated approach to rolling contact sub-surface fatigue assessment of railway wheels. *Wear* 258 (2005), pp. 973–980.

[14] J.W. Ringsberg: Life prediction of rolling contact fatigue crack initiation. *Int. J. Fat.* 23 (10) (2001), pp. 575-586.

[15] S. Bari, T. Hassan: Anatomy of coupled constitutive models for ratcheting simulations. *Int. J. Plast.* 16 (3-4) (2000), pp. 381-409.

[16] A. Kapoor: Wear by plastic ratchetting. *Wear* 212 (1) (1997) pp. 119-130.

[17] A. Kapoor: A re-evaluation of the life to rupture of ductile metals by cyclic plastic strain. *Fatigue & Fracture of Engineering Materials & Structures* 17 (1994), pp. 201-219.

[18] P. Clayton, X. Su: Surface Initiated fatigue of pearlitic and bainitic steels under water lubricated rolling/sliding contact. *Wear* 200 (1996), pp. 63-73.

[19] X . Su, P. Clayton: Ratchetting strain experiments with a pearlitic steel under rolling/sliding contact. *Wear* 205 (1997), pp. 137-143.

[20] K. Mitura, R. Faja, P.Matušek, R.Fajkoš: Catalogue of wheel set defects rising during its service life, Technical Handbook for Wheel Set Keepers No. 25-271 (3rd edition), BONATRANS GROUP, Revolucni 1234, Bohumin, Czech republic, 236 pp. (in Czech)

[21] A. Mazzú, G. Donzella, M. Faccoli, C. Petrogalli, R. Roberti: Progressive damage assessment in the near-surface layer of railway wheel-rail couple under cyclic contact. *In Proc. of the 8th International Conference on Contact Mechanics and Wear of Rail/Wheel Systems (CM2009)*, September 15-18, 2009, Italy, pp.99-104.

[22] M. Abdel-Karim, N. Ohno: Kinematic hardening model suitable for ratchetting with steady-state. *Int. J. Plast.*16 (3-4) (2000), pp. 225-240.

[23] R. Halama: A modification of abdelkarim-ohno model for ratcheting simulations. *Technical Gazette* 15 (3) (2008), pp. 3-9.

[24] R. Halama, F. Fojtík, J. Brumek, M. Fusek: Ratcheting measurement during fatigue testing. *In Proc. of International Conference Applied Mechanics 2009*, April 6-8, 2009, Slovakia, pp.43-44.

[25] M. Kobayashi, N. Ohno: Implementation of cyclic plasticity models based on a general form of kinematic hardening. *Int. J. Numer. Meth. Engng* 53 (2002), pp. 2217-2238.

[26] R. Halama: Rolling contact simulations with various cyclic plasticity models. *In Proc. of Ansys Conference & 25th CADFEM Users' Meeting, Dresden: CADFEM GmbH*, November 21-23, 2007, (CD-ROM).

[27] D.L. McDowell: Stress state dependence of cyclic ratchetting behavior of two rail steels. *Int. J. Plast.* 11 (4) (1995), pp. 397-421.

[28] J.W. Ringsberg: Shear mode growth of short surface-breaking RCF cracks. *Wear* 258 (2005), pp. 955-963.

[29] Y. Liu, L. Liu, S. Mahadevan: Analysis of subsurface crack propagation under rolling contact loading in railroad wheels using FEM. *Engineering Fracture Mechanics* 74 (2007), pp. 2659–2674.

Appendix A: Notation

a	half width of contact area
$\mathbf{a}$	deviatoric part of back stress
C	material constant
D_{LCF}	damage caused by low-cycle fatigue
D_R	damage caused by ratcheting
f	traction coefficient

$\overline{f}$	yield function
F	total normal contact force
FP	fatigue parameter
FP_0	material fatigue constant
$H(f_i)$	Heaviside's step function
J	material fatigue constant
k	shear yield stress
K	material fatigue constants
m	material fatigue constant
M	number of back stress parts
N	number of cycles
N_f	number of cycles to fatigue crack initiation
N_w	number of cycles to constant wear rate conditions
p	equivalent plastic strain
p_0	Hertzian contact pressure
$\overline{p_0}$	maximum of applied normal contact stresses
R_a	roughness
$\mathbf{s}$	deviatoric part of stress tensor
x	distance from the pressure peak
z	depth measured from the contact surface
α	back stress
ε_p	plastic strain tensor
ε_x	axial strain
ε_{xa}	magnitude of axial strain
$\Delta\varepsilon$	normal strain range
γ	material constant
γ_{cri}	critical value of the accumulated shear strain
γ_r	shear ratcheting strain
$\Delta\gamma$	shear strain range
μ	ratcheting parameter
μ_0	material constant
μ_∞	material constant
σ	stress tensor
σ_{max}	maximal stress
σ_x	axial stress
σ_{xa}	magnitude of axial stress
σ_{xm}	mean axial stress
σ_Y	size of a yield surface
ω	material constant
τ_{xy}	shear stress component
τ_a	magnitude of shear stress
$\Delta\tau$	shear stress range

Figures

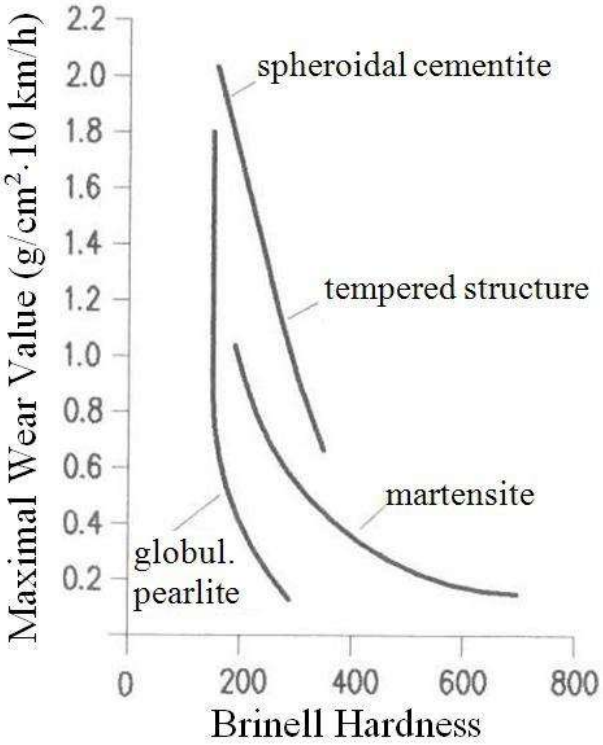

Fig. 1. Wear values as function of Brinell hardness and microstructure morphology

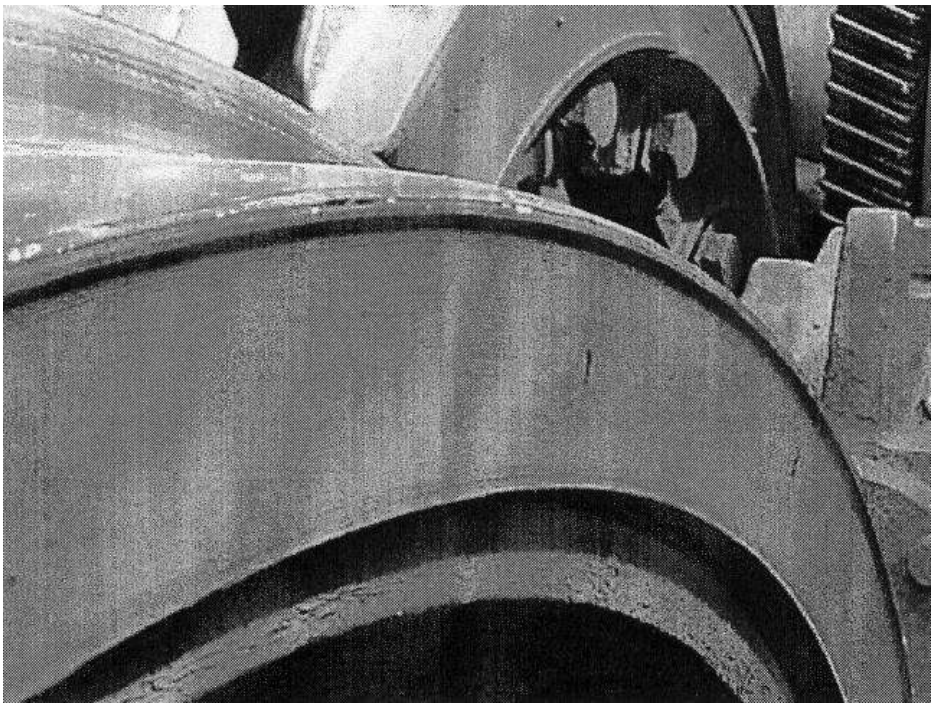

Fig.2. A photo of outer rim edge rollover

Wear. 2011, vol. 271, issue 1-2, p. 174-185. Elsevier http://dx.doi.org/10.1016/j.wear.2010.10.053

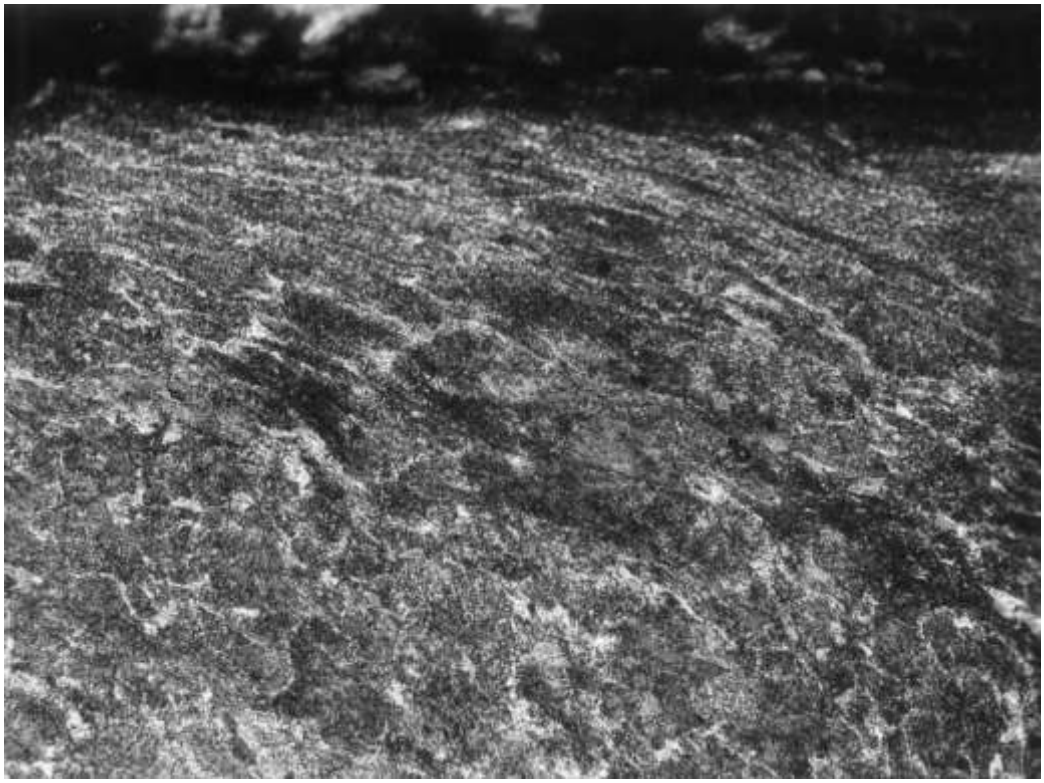

Fig.3. Thermal affection of surface layer and plastic deformation in the direction from the running surface to the rim face (magnification 500 x)

Fig. 4. Defect of pitting type on the wheel tread

Wear. 2011, vol. 271, issue 1-2, p. 174-185. Elsevier http://dx.doi.org/10.1016/j.wear.2010.10.053

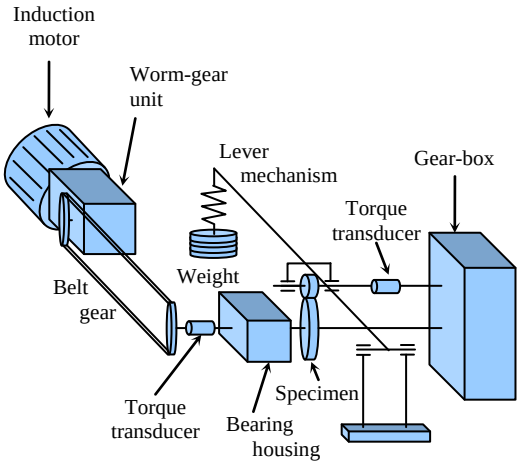

Fig. 5. Schematic representation of the TUORS machine

Fig. 6. A photograph of a specimen from the test realization

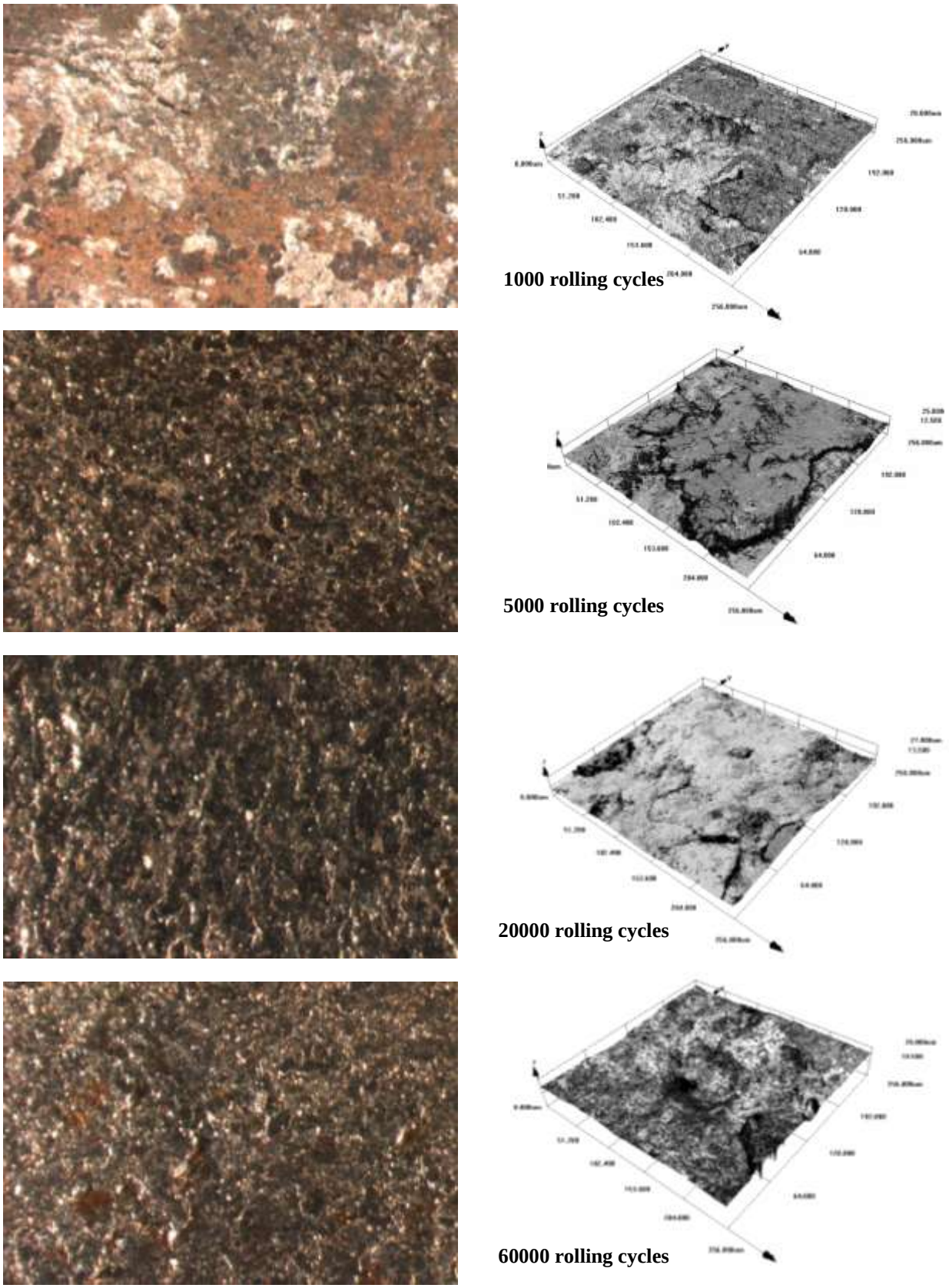

Fig.7. Surface photo-documentation of chosen specimens by the stereo-microscope (left) and by the confocal microscope

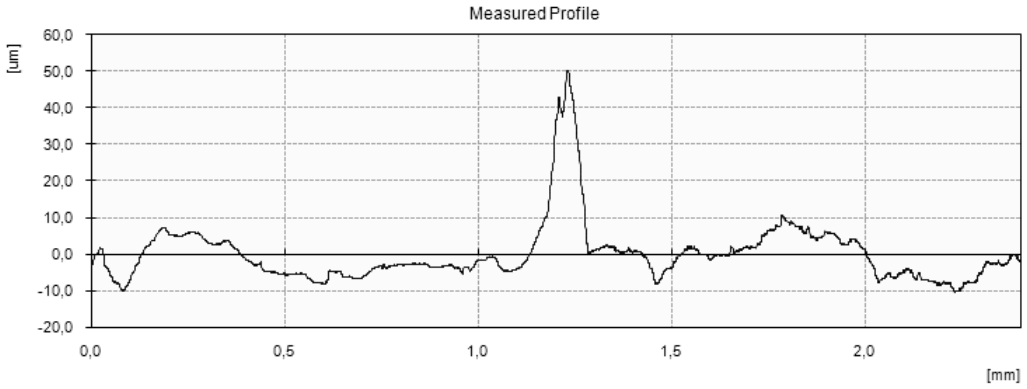

Fig. 8. Sample of roughness measurement

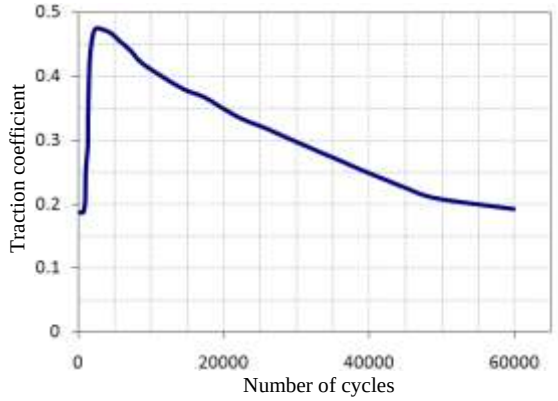

Fig. 9. Graph of the traction coefficient and number of cycles for the test with the longest rolling distance

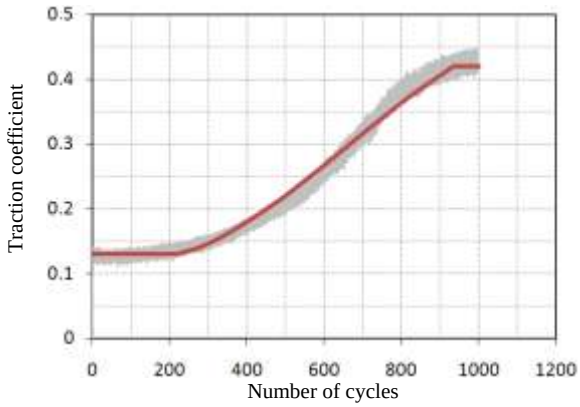

Fig. 10. The dependence of the traction coefficient and the number of cycles for the test with 1000 rolling cycles

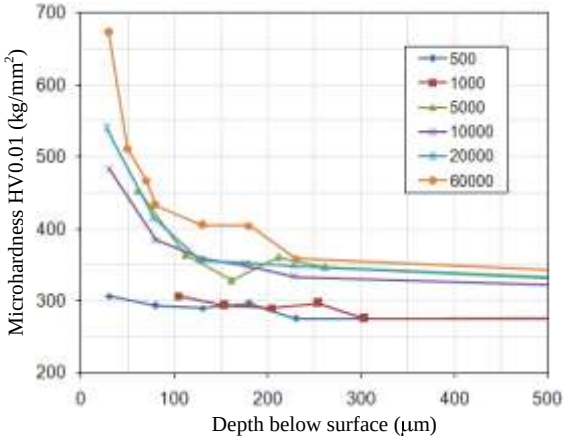

Fig. 11. Dependence between microhardness HV0.01 and the depth under surface for particular specimens

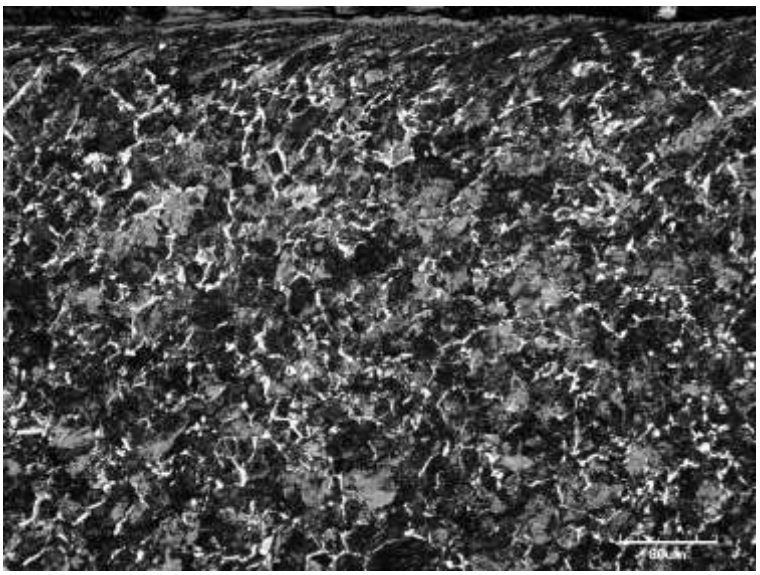

Fig. 12. Deformed structure below the contact surface after 1000 cycles

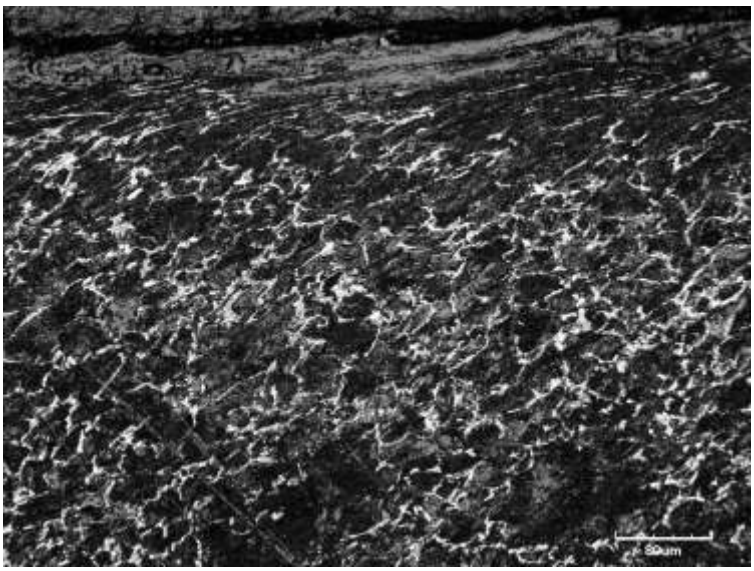

Fig. 13. Deformed structure below the contact surface after 5000 cycles

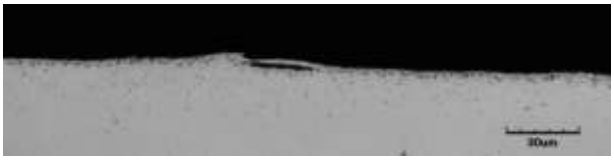

500 rolling cycles

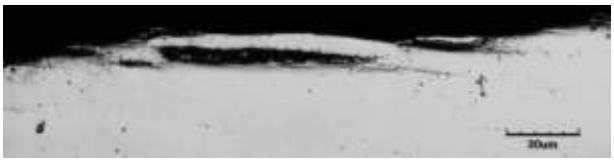

1000 rolling cycles

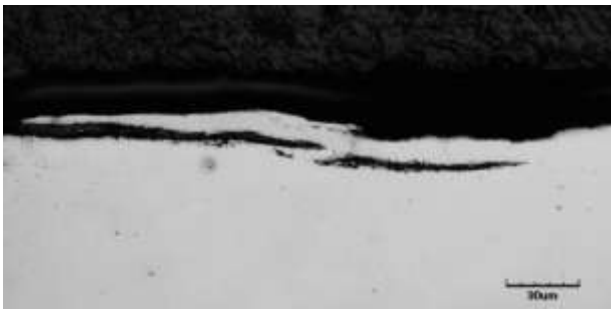

5000 rolling cycles

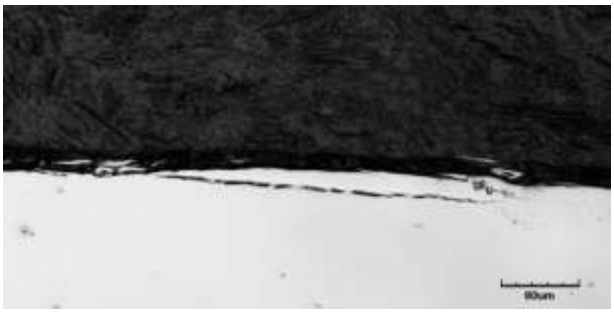

10000 rolling cycles

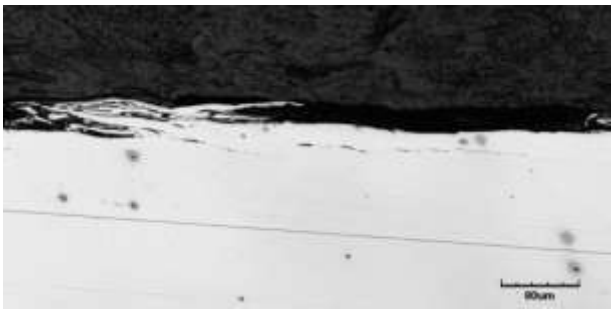

20000 rolling cycles

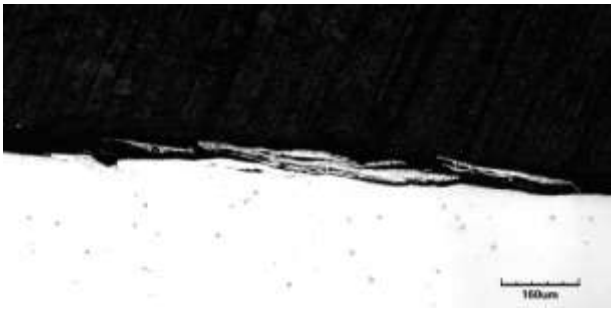

60000 rolling cycles

Fig. 14. Characteristic surface damage in different phases of contact defect rise

Wear. 2011, vol. 271, issue 1-2, p. 174-185. Elsevier http://dx.doi.org/10.1016/j.wear.2010.10.053

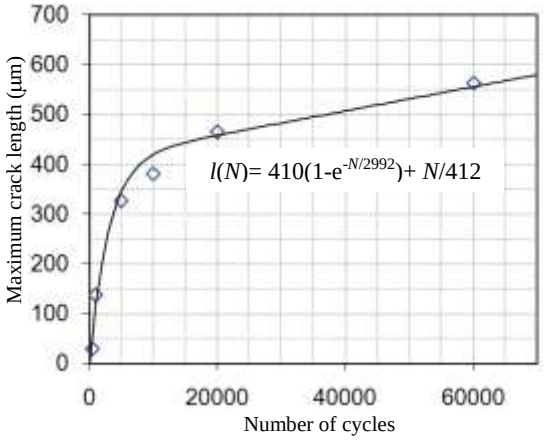

Fig. 15. Evaluated dependence between the crack length and the number of cycles

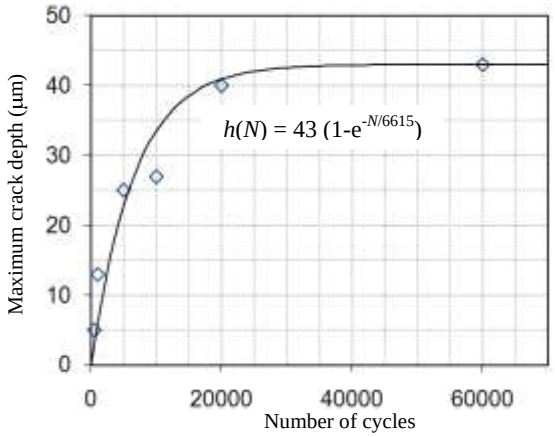

Fig. 16. Evaluated dependence between the crack depth and the number of cycles

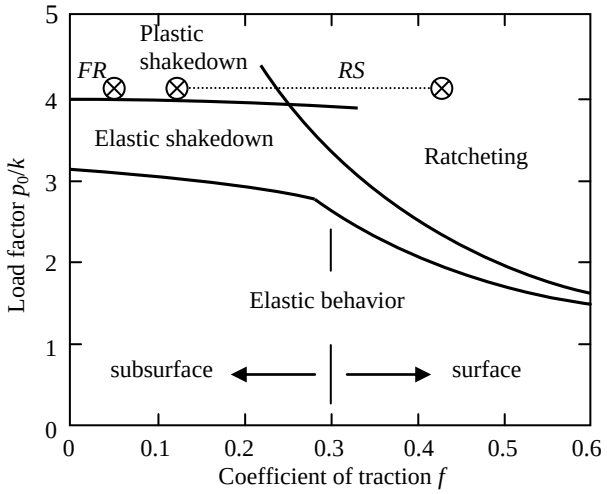

Fig. 17. Shakedown map of the line rolling contact case

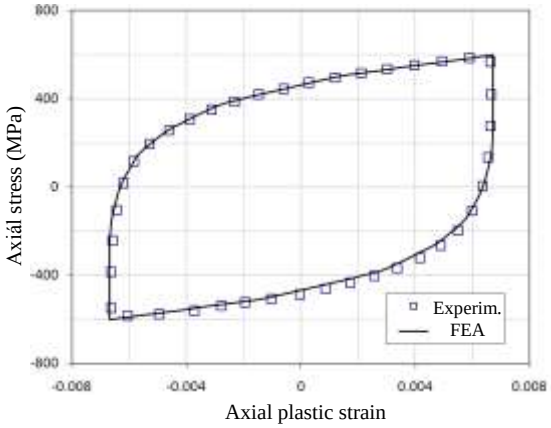

Fig. 18. Uniaxial stable hysteresis loop: experiment (squares) and simulation

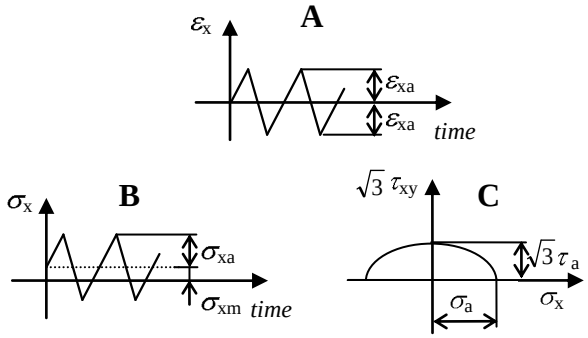

Fig. 19. The scheme of three realized loading paths

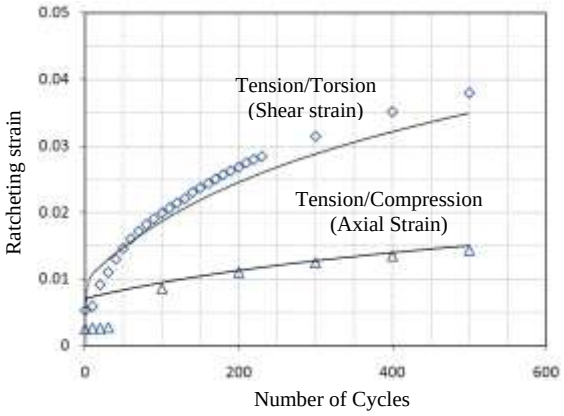

Fig. 20. Axial ratcheting strain as a function of cycles for the case B (experiment- triangles, prediction- solid curve) and shear ratcheting strain as a function of cycles for the case C (experiment- squares, prediction-solid curve)

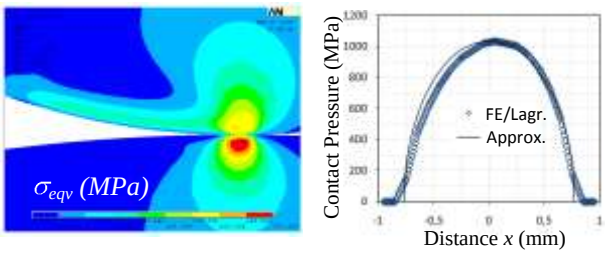

Fig. 21. Rolling contact simulation by the Augmented Lagrangian method: von Mises equivalent stress contours (left), contact pressure from FE analysis and its approximation by the Hertzian function (right)

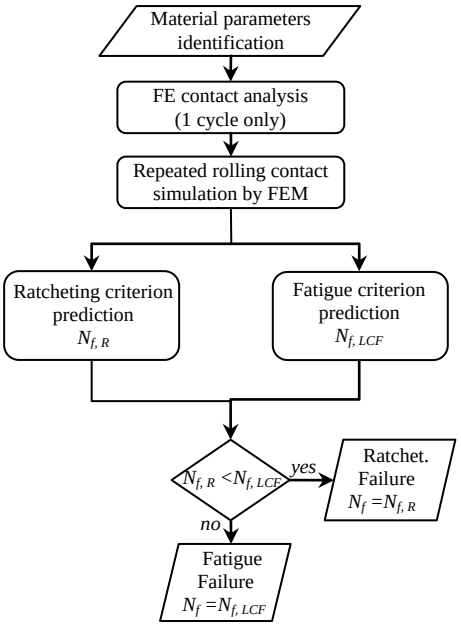

Fig. 22. Used strategy for prediction of fatigue crack initiation

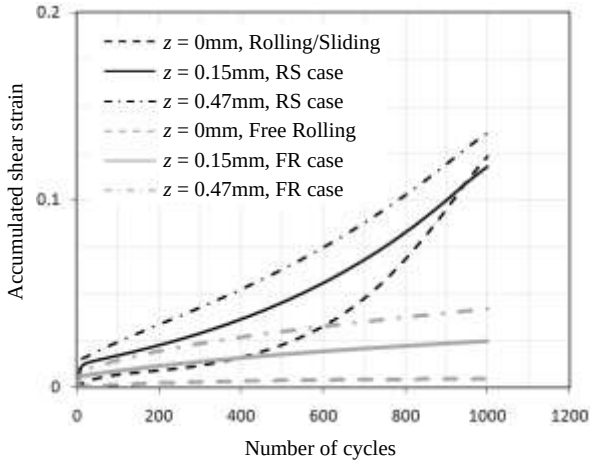

Fig. 23. Dependence between the accumulated shear strain and the number of cycles for three locations from both FEAs

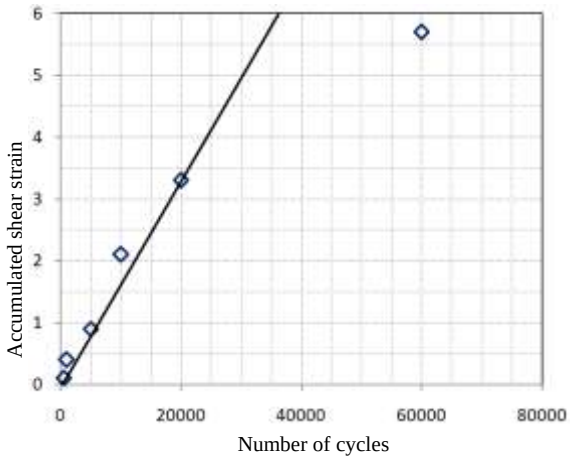

Fig. 24. Comparison of strain accumulation at the point 0.15 mm below the contact surface: prediction by the FE method (solid line) and measurement (squares)

Tables

Table 1 Extract from the catalogue of wheelset defects [20]

Defect localisation	Defect ID	Defect type	Probable cause
Wheel tread	WR 216	Pitting on wheel tread	Contact cyclic loads of the wheel tread, temperature loading under breaking and rolling/sliding
	WR 217	Wheel flats combined with pitting on wheel tread	
	WR 221	Transverse cracks on wheel tread	Breaking heat from shoe brakes, plastic deformation of surface layer
	WR. 222	Oblique crack on wheel tread	
	WR 211	Slip-creepage	Wheelset leading in wheel frame, properties of track and slide protection
	WR 223	Crack networks on wheel tread	Wheel heating under stop braking and consequential quick wheel tread cooling
	WR 224	Cracks on outer side of wheel-crown – thermal cracks	Brake shoe offset through rim face
	WR 225	Thermal cracks on wheels braking by brake on rim face	Thermal loading under braking through rim face
	WR 233	Wheel fracture coming out of field side chamber	Brake shoe offset through rim face, overheating, dynamic loads, fatigue process
	WR 241	Slots on wheel tread	Brake shoe offset
	WR 242	Grooves, comb indentation on wheel tread	Wheel tread warming-up under braking, abrasive material on break shoe
	WR 243	Abnormal wear of wheel tread	Wear mechanisms, hard surface layers of brake shoes causing wheel abrasion
	WR 244	Flange tip rollover	
	WR 2411	Wheel overloading (excessive strains or stresses)	Wheel overheating, substantial redistribution of residual stresses
	WR 251	Glue-on material on wheel tread	Bad settings of braking system, improper material of brake shoe

Table 2 Test conditions and main test results

	Number of revolutions					
	500	1000	5000	10000	20000	60000
Surface roughness at the end of test R_a (µm)	1.04	1.98	1.69	1.95	2.58	2.89
Coefficient of traction:						
-Maximum	0.193	0.437	0.452	0.469	0.455	0.474
-End of test	0.193	0.437	0.404	0.413	0.336	0.193
Total disc weight loss (g):						
Wheel (R7T)	0.02	0.02	0.12	0.26	0.3	2.32
Rail (Class C)	>0.01	>0.01	0.06	0.14	0.2	1. 05
Disc diameter loss (mm)	0.023	0.11	0.292	0.321	0.364	0.621
Change of track width (mm)						
Wheel (R7T)	0.195	0.213	0.592	0.805	0.95	1.319
Rail (Class C)	0.006	0.257	0.531	0.716	0.886	1.587
Maximum crack length/depth (µm)	30/5	137/13	326/25	380/27	466/40	563/43
Shear strain 0.15mm below the contact surface	0.1	0.4	0.9	2.1	3.3	5.7

Table 3 Material parameters of AbdelKarim-Ohno model for R7T steel

Material parameters
$E = 180000\,MPa$, $\nu = 0.3$, $\sigma_Y = 200\,MPa$
$C_{1-6} = 310600, 130770, 53290, 32420, 12940, 1850\,MPa$
$\gamma_{1-6} = 5884, 2020, 980, 520, 255, 3$
$\mu_0 = 0.5, \omega = 0.5, \mu_\infty = 0.14$

Table 4 Material fatigue and ratcheting properties of R7T steel

	Material parameters
LCF model parameters	$J = 0.37$, $FP_0 = 0.55$, $K = 23400$, $m = 1.9$
Ratcheting parameter	$\gamma_{cri} = 0.35$

Table 5 Resulting number of cycles to crack initiation

	Critical plane approach (Jiang-Sehitoglu)		Ratcheting criterion (Kapoor)	
	N_f	Depth (mm)	N_f	Depth (mm)
RS case	4 933	0	**1 366**	0
FR case	**15 112**	0,42	39 635	0,42